JCTC Journal of Chemical Theory and Computation

pubs.acs.org/JCTC Article

NEXMD Software Package for Nonadiabatic Excited State Molecular Dynamics Simulations

Walter Malone, Benjamin Nebgen, Alexander White, Yu Zhang, Huajing Song, Josiah A. Bjorgaard, Andrew E. Sifain, Beatriz Rodriguez-Hernandez, Victor M. Freixas, Sebastian Fernandez-Alberti, Adrian E. Roitberg, Tammie R. Nelson,* and Sergei Tretiak*

Cite This: *J. Chem. Theory Comput.* 2020, 16, 5771−5783 Read Online

ACCESS | Metrics & More | Article Recommendations | Supporting Information

ABSTRACT: We present a versatile new code released for open community use, the nonadiabatic excited state molecular dynamics (NEXMD) package. This software aims to simulate nonadiabatic excited state molecular dynamics using several semiempirical Hamiltonian models. To model such dynamics of a molecular system, the NEXMD uses the fewest-switches surface hopping algorithm, where the probability of transition from one state to another depends on the strength of the derivative nonadiabatic coupling. In addition, there are a number of algorithmic improvements such as empirical decoherence corrections and tracking trivial crossings of electronic states. While the primary intent behind the NEXMD was to simulate nonadiabatic molecular dynamics, the code can also perform geometry optimizations, adiabatic excited state dynamics, and single-point calculations all in vacuum or in a simulated solvent. In this report, first, we lay out the basic theoretical framework underlying the code. Then we present the code's structure and workflow. To demonstrate the functionality of NEXMD in detail, we analyze the photoexcited dynamics of a polyphenylene ethynylene dendrimer (PPE, $C_{30}H_{18}$) in vacuum and in a continuum solvent. Furthermore, the PPE molecule example serves to highlight the utility of the *getexcited.py* helper script to form a streamlined workflow. This script, provided with the package, can both set up NEXMD calculations and analyze the results, including, but not limited to, collecting populations, generating an average optical spectrum, and restarting unfinished calculations.

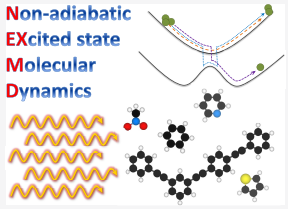

INTRODUCTION

The fast-paced modern technological landscape increasingly demands the design of new materials with desired functionalities. In particular, photoactive functional materials are of interest in organic light-emitting diodes,[1] photovoltaics,[2−6] field-effect transistors,[7,8] sensors,[9−12] and photocatalysts,[13] to name a few. For this purpose, organic conjugated materials (OCMs), such as polymers, small molecules, molecular crystals, and donor−acceptor systems, are commonly used as photoactive semiconductor materials.[14,15] Delocalized and polarizable π-electrons endow these materials with desirable electronic properties and allow for mobile charge carriers.[16] As revealed by optical experiments, OCMs exhibit complex excited state electronic structure due to their low dimensionality and strong electronic correlations.[17] Similar properties are common for many other molecular electronic materials such as biological chromophores (retinals, fluorescent proteins, chlorophylls, and carotenoids) underpinning many natural processes, for example, vision, bioluminescence, and photosynthesis.[12,18−22] In all these materials, the dynamics of electronic excitations is dominated by significant nonadiabatic (NA) couplings through a breakdown of the Born−Oppenheimer (BO) approximation. Following photoexcitation, various nonradiative intraband relaxation pathways can lead to a number of complex photoinduced processes such as internal conversion, energy transfer, charge separation, and spatial localization of excitons,[23−25] as well as photochemical reactions or isomerization.[26,27] Computational simulation of nonadiabatic molecular dynamics (NAMD) is an indispensable tool for understanding and controlling optoelectronic properties and photoinduced pathways. Thus, nonadiabatic processes play a central role in many technological applications, atmospheric,[28] environmental,[29] and biological chemistry,[20,30,31] among others. As such, many software packages implement various approaches for NAMD.[32−39]

Adiabatic or BO molecular dynamics (BOMD), in which trajectories are propagated along a single molecular potential energy surface (PES) of a ground[40] or excited state,[41,42] are valuable for modeling the ultrafast dynamics of excited electron-vibrational states on femtosecond to nanosecond timescales in large organic molecules (nanometer length scales).[43,44] When dynamics becomes nonadiabatic, electronic and nuclear motions can no longer be separated and the BO approximation fails.[45] Nonadiabatic processes occur when excited state PESs become energetically close or cross.[46] In this

Received: March 13, 2020
Published: July 8, 2020

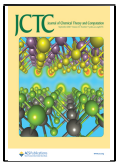

https://dx.doi.org/10.1021/acs.jctc.0c00248
J. Chem. Theory Comput. 2020, 16, 5771−5783

regime, one must go beyond the BO approximation using fully quantum,[47,48] semiclassical,[49−57] or mixed quantum-classical (MQC)[58−61] approaches to describe NAMD. While the fully quantum and semiclassical methods provide high accuracy results, they are generally too expensive to apply to extended molecular systems that often contain hundreds of atoms and involve large densities of excited states participating in the photoinduced dynamics. Alternatively, the molecular dynamics with quantum transitions (MDQT) method, particularly the fewest-switches surface hopping (FSSH) approach,[62] is one of the most widely used MQC methods for NAMD simulations.

Our group has developed the nonadiabatic excited state molecular dynamics (NEXMD) software package, which utilizes the semiempirical quantum mechanics (SQM) package from AmberTools[63] to implement an efficient framework to describe photoinduced phenomena in extended conjugated molecular systems. The NEXMD code can perform both BOMD and NAMD simulations. For the latter, we use the FSSH algorithm within an adiabatic basis to treat quantum transitions among multiple excited states. The time-dependent Hartree−Fock (TD-HF)[64−66] or the configuration interaction singles (CIS)[65,67] level of theory can be combined with a semiempirical Hamiltonian to provide a sufficiently fast and accurate description of the excited state manifold in relatively large molecular systems. Analytical techniques remove the computational barrier to computing the complete set of NA couplings[68,69] and allow excited state gradients[70−72] to be computed on-the-fly. This allows for dynamical propagation on the native excited state PES, going beyond the classical path approximation (CPA).[73] Furthermore, solvation effects arising from electrostatic screening can be incorporated via implicit continuum solvent models.[74] Finally, well-known deficiencies of the FSSH algorithm are overcome by correcting for trivial unavoided crossings and decoherence.[75−77] Thus, the NEXMD code offers a variety of functionalities for both BOMD and NAMD simulations in realistically large (hundreds of atoms) molecular systems propagated on timescales up to tens of picoseconds.

The utility and accuracy of the NEXMD development version were exemplified by its application to a variety of systems including oligomers and polymers,[78−89] dendrimers,[90−94] light harvesting complexes (LHCs),[18,19,95] energetic materials,[96−98] and others.[99] Additionally, our previous publications documented the development of theoretical methodology, algorithms, and analyses featured in NEXMD.[75−77,81,100−104] In this article, we outline the various functionalities of the NEXMD package derived from the development version and released for open public use and the associated *getexcited.py* python support package. The *getexcited.py* scripts contain tools for generating initial conditions, computing optical spectra, populating initial excited states, and performing data analysis. We then demonstrate the features of NEXMD and various analyses available in the *getexcited.py* package with application to modeling photoexcited energy transfer dynamics in a model polyphenylene ethynylene (PPE) dendrimer.[105] The paper is organized as follows: Section 2 covers the theoretical methodology employed in the NEXMD software and highlights different dynamics capabilities currently available. In Section 3, we discuss the code structure and workflow for setting up and running a typical simulation. Section 4 exemplifies the NEXMD simulations of photoexcited dynamics in a model PPE dendrimer with emphasis on various developed analysis techniques. Finally, our conclusions are presented in Section 5.

THEORETICAL METHODOLOGY

Electronic Structure Calculations. For the ground state electronic structure description, NEXMD ultizes the Hartree−Fock (HF) method. The software package interfaces with the SQM quantum chemistry program[106] in AmberTools, which provides a variety of semiempirical Hamiltonians such as Austin Model 1 (AM1),[107] Parameterized Model number 3 (PM3),[108] MNDO/d,[109] and Parameterized Model number 6 (PM6),[110] among others. At each self-consistent field (SCF) iteration, the initial guess to subsequent SCF steps is calculated using combinations of ground state configurations from previous SCF steps. The ground state convergence criteria specify the minimum energy difference between two SCF steps before convergence is achieved following the SQM implementation.[106]

Excited states can be calculated using either configuration interaction singles (CIS) or time-dependent Hartree−Fock (TD-HF), also known as the first-order random phase approximation (RPA). Both methods rely on the collective electron oscillator (CEO) approach[111,112] to solve the TD-HF equation of motion[67] for the single electron density matrix.[113] We define the single electron density matrices for the adiabatic electronic eigenstates $|\phi\rangle$ of the system (solutions of the time-independent electronic Schrödinger equation) labeled by α and β as

$$(\rho_{\alpha\beta})_{mn} = \langle \phi_\alpha | c_m^\dagger c_n | \phi_\beta \rangle \tag{1}$$

where n and m denote the atomic orbital (AO) basis functions and $c_m^\dagger$ and c_m are electronic creation and annihilation operators, respectively. Here and throughout, we use the following notations: ground and excited states of a molecule are well-defined, and their energies/many-body wave functions depend parametrically on the set of nuclear coordinates $\boldsymbol{R}$ (e.g., $E_0(\boldsymbol{R})/\phi_0(\boldsymbol{R})$ and $E_\alpha(\boldsymbol{R})/\phi_\alpha(\boldsymbol{R})$ for the ground and excited states, respectively). Then, the eigenfunctions of the tetradic Liouville operator L[72,112]

$$L\xi_\alpha = \Omega_\alpha \xi_\alpha \tag{2}$$

correspond to the transition density matrices $\xi_\alpha = \rho_{0\alpha}$, which describe the change in density induced by the ground to excited state transitions $|0\rangle \rightarrow |\alpha\rangle$. The eigenvalues Ω_α are the respective electronic transition energies such that the excited state energy of state α is given by the ground state SCF energy plus the transition energy as $E_\alpha = E_0 + \Omega_\alpha$. Equation 2 can be written in matrix form in the molecular orbital (MO) basis as[72]

$$\begin{pmatrix} A & B \\ -B & -A \end{pmatrix} \begin{bmatrix} X \\ Y \end{bmatrix} = \Omega \begin{bmatrix} X \\ Y \end{bmatrix} \tag{3}$$

which is the RPA eigenvalue equation.[67] The transition density matrix $\xi = \begin{bmatrix} X \\ Y \end{bmatrix}$ consists of X and Y components corresponding to the particle-hole and hole-particle subparts,[72,112] respectively. The CIS approximation neglects B in eq 3[114] resulting in

$$AX = \Omega X \tag{4}$$

where the Hermitian matrix A is the CIS matrix. The TD-HF (RPA) approach includes the de-excitation operator (matrix B) in eq 3, but the method is more computationally expensive.

https://dx.doi.org/10.1021/acs.jctc.0c00248
J. Chem. Theory Comput. 2020, 16, 5771−5783

The Davidson diagonalization algorithm[114−117] is used to solve eq 3 (TD-HF) or 4 (CIS) for the excitation energies Ω_α at approximately $O(N^3)$ cost, where N is the number of AO orbitals considered in the system. For N_S requested excited states, the Davidson algorithm implemented in NEXMD solves for $N_S + 1$ eigenstates in order to improve the accuracy of the highest value transition (N_S).[118]

Geometry Optimization and Gradients. Calculation of forces (or energy gradients) on each atom for a given potential energy surface performed using the Hellmann−Feynman theorem[119,120] underpins all geometry optimizations, as well as BOMD and NAMD simulations described below. Both ground and excited state energy gradients

$$\frac{\partial E_\alpha(\boldsymbol{R})}{\partial \boldsymbol{R}} = \frac{\partial E_0(\boldsymbol{R})}{\partial \boldsymbol{R}} + \frac{\partial \Omega_\alpha(\boldsymbol{R})}{\partial \boldsymbol{R}} \tag{5}$$

are computed analytically, which is a superior approach to numerical derivatives. We refer the reader to refs 70, 72 and 100 for a more detailed description.

Geometry optimization then uses the basic steepest descent (or gradient descent) procedure that relaxes the structure iteratively by moving the atoms down the energy gradient until a sufficiently low average gradient (force) is obtained. Both the force criterion (minimization is converged when forces are smaller than a specified value) and a maximum number of geometry optimization cycles can be specified. In the current NEXMD release version, all atomic coordinates are included in the minimization routine, and no vibrational degrees of freedom can be frozen. For any specific nuclear configuration, a single point calculation of the electronic structure can be performed to obtain various ground or excited state properties. Table 1 provides an overview of the different types of calculations/dynamics available in the NEXMD and various features that are supported within each category.

Solvent Models. The interaction of the system (solute) with the environment (solvent) can significantly alter the optical properties and influence the photoinduced dynamics.[121] While the solute is treated quantum-mechanically, one can treat the solvent either explicitly using molecular mechanics (a family of so-called QM/MM methods)[122] or implicitly using a range of continuum solvation models.[74] The latter avoids explicit treatment of solvent degrees of freedom and maintains a minimal system size. However, these methods do account for long-range electrostatic interactions contributing to many solvation effects and include the effect of electronic polarization of the solute.[74] In NEXMD, we use the implicit self-consistent reaction field (SCRF) models.[123] Here, the continuum solvent generates a reaction field (i.e., solvent potential) that depends on the electron density of the solute and is therefore iterated self-consistently during the wave function convergence. The available potentials include either the Onsager model[124,125] or the conductor-like screening model (COSMO).[126] For the Onsager model, the solvent is modeled as a polarizable medium with a continuous dielectric constant, ε, and the solute is placed inside a spherical solvent cavity with a specified radius. COSMO is a more sophisticated model where a refined molecule-shaped cavity is used.

The effective solvent potential describes the electrostatic interaction between the charge densities of the solute and solvent. For excited states, several methods for describing the mutual polarization involving the excited state density have been developed over the years. In the linear response (LR) method,[127−129] the transition density polarizes the solvent, which allows for the sequantial solution of the ground state SCF equation followed by the solution of the RPA eigenvalue equation. However, the LR model is limited to cases where the excited state has a substantial transition dipole moment and a permanent dipole moment similar to the ground state. The absence of interactions with excited state charge density in LR precludes description of states with dissimilar permanent dipole moments such as charge-transfer transitions. The state-specific (SS) solvation model[130,131] addresses this deficiency by including excited state polarization, where the electronic density of a specific state polarizes the solvent potential. However, this requires an iterative solution of both SCF and RPA equations and is numerically expensive. A third option, the vertical excitation (VE) model,[132] provides an approximate solution to the SS model and can be solved by a self-consistent iteration with only a single RPA diagonalization.

For more details about the implementation of these models in NEXMD, we refer to our previous publications.[102,103] Importantly, only LR and VE models allow formulation of excited state analytic gradients. The LR model permits all calculations listed in Table 1. The VE model is available only for excited state single-point calculations and geometry optimizations, as well as excited state BOMD. Finally, the

Table 1. NEXMD Functionalities, Represented by Columns, and the Different Features Available for Each Functionality, Represented by Rows[a]

	geometry optimization (GS or ES)	single point (GS or ES)	adiabatic BOMD (GS or ES)	NAMD
total molecular dipole	X*	X*		X
transition dipole (GS to ES)	X*	X*	X*	X
transition dipole (ES to ES)		X*		
difference dipole relaxed/ unrelaxed	X*	X*		X
Mulliken charges	X	X	X	X
CIS	X	X	X	X
RPA (TD-HF)	X	X	X	X
restart Davidson from previous guess	X*		X*	X
LR solvent model	X	X	X	X
VE solvent model	X*	X*	X*	
SS solvent model		X*		
COSMO potential	X	X	X	X
Onsager potential	X	X	X	X
electric field	X	X	X	X
instantaneous decoherence				X
trivial crossing				X
Newtonian dynamics (NVE)			X	X
Langevin dynamics (NVT)			X	X
analytical gradients			X	X
analytical NAC				X

[a]X denotes an available option. * denotes an option that is available only for the excited state calculations.

https://dx.doi.org/10.1021/acs.jctc.0c00248
J. Chem. Theory Comput. 2020, 16, 5771−5783

full SS model can be used only for excited state single-point calculations owing to the absence of gradients. Moreover, a static external electric field can also be applied for any type of calculation listed in Table 1.

Nuclear Propagation, Thermostat, and Adiabatic Molecular Dynamics. For both BOMD and NAMD simulations, nuclei are treated classically and propagated using a numerical velocity Verlet (VV) finite difference algorithm.[133,134] MD can be performed via the constant energy microcanonical ensemble (NVE) or constant temperature canonical ensemble (NVT). For NVE simulations, the Newtonian equation of motion is integrated for the nuclei

$$M_i\ddot{\boldsymbol{R}}_i(t) = -\nabla E_\alpha(\boldsymbol{R}(t)) \tag{6}$$

where M_i, $\ddot{\boldsymbol{R}}_i$, and $\boldsymbol{R}_i$ give the mass, acceleration, and position of the ith nucleus, respectively. Instead, for NVT simulations, the constant temperature Langevin equation of motion is used

$$M_i\ddot{\boldsymbol{R}}_i(t) = -\nabla E_\alpha(\boldsymbol{R}(t)) - \zeta M_i\dot{\boldsymbol{R}}_i(t) + \boldsymbol{A}(t) \tag{7}$$

Here, $\dot{\boldsymbol{R}}_i(t)$ is the velocity of the ith nucleus, and ζ (ps^{-1}) is the friction coefficient. $\boldsymbol{A}$ is the stochastic force related to the bath temperature T through the fluctuation−dissipation relation[135] $\langle \boldsymbol{A}_i(t) \cdot \boldsymbol{A}_i(t + \Delta t)\rangle = 2M_i\zeta k_B T\delta(\Delta t)\delta_{ij}$, where k_B is the Boltzmann constant, $\delta(\Delta t)$ is the Dirac delta function, δ_{ij} is the Kronecker delta function, and $\langle\rangle$ signifies the equilibrium time average. Langevin dynamics is implemented using an algorithm consistent with VV integration[136] and uses a random number generator[137] for the stochastic force.

Nonadiabatic Molecular Dynamics (NAMD). *The Fewest-Switches Surface Hopping Algorithm.* NAMD simulations go beyond the BO approximation by allowing quantum transitions between coupled excited states. To achieve this, NEXMD implements the FSSH approach.[62] In this method, an ensemble of M independent trajectories is propagated. Within each trajectory, the electronic degrees of freedom are treated quantum mechanically while the nuclear coordinates are propagated classically according to the forces from a single adiabatic PES, and the trajectory can transition (hop) to a different electronic state depending on the strength of the nonadiabatic (NA) coupling. In practice, NVT (eq 7) is typically used for ground state adiabatic dynamics to sample the conformational space and generate initial geometries and momenta used for subsequent NAMD simulations performed using NVE (eq 6) dynamics. While the nuclear trajectory evolves on the current adiabatic state labeled α, the electronic wave function is expressed as a mixture of adiabatic basis functions ϕ_i (eigenstates of the adiabatic Hamiltonian)

$$\Psi(\boldsymbol{R}, t) = \sum_i c_i(t)\phi_i(r; \boldsymbol{R}) \tag{8}$$

where r is the electronic degree of freedom and $c_i(t)$ are the time-dependent adiabatic expansion coefficients. These coefficients contain a parametric dependence on $\boldsymbol{R}$. The equation of motion for these coefficients follows the time-dependent Schrödinger equation to give

$$i\hbar\frac{\partial c_i(t)}{\partial t} = c_i(t)E_i(\boldsymbol{R}) - i\hbar\sum_j c_j(t)\dot{\boldsymbol{R}}\cdot\boldsymbol{d}_{ij} \tag{9}$$

where $\boldsymbol{d}_{ij}$ is the NA coupling vector (NACR) defined as $\boldsymbol{d}_{ij} = \langle\phi_i \mid \nabla\phi_j\rangle$ for $i \neq j$, $\boldsymbol{d}_{ii} = 0$, and $\boldsymbol{d}_{ij} = -\boldsymbol{d}_{ji}$. The time-dependent scalar product (NACT) is given by $\dot{\boldsymbol{R}}\cdot\boldsymbol{d}_{ij} = \langle\phi_i|\frac{\partial\phi_j}{\partial t}\rangle$. NACR and NACT are computed analytically[68,69] as

$$\boldsymbol{d}_{ij} = \frac{Tr(F^{(R)}\rho_{ij})}{\Omega_i - \Omega_j},\ i \neq j \tag{10}$$

$$\dot{\boldsymbol{R}}\cdot\boldsymbol{d}_{ij} = \frac{Tr(F^{(t)}\rho_{ij})}{\Omega_i - \Omega_j} \tag{11}$$

where superscripts (R) and (t) denote the respective derivatives of the Fock matrix elements.

The coefficients $c_i(t)$ define the time-dependent density matrix with elements given by $a_{ij}(t) = c_i^*(t)c_j(t)$. The probability that a hop from the current adiabatic state α to another state β will occur during the time interval Δt is given by

$$g_{\alpha\beta} = \Delta t\frac{b_{\beta\alpha}(t)}{a_{\alpha\alpha}(t)} \tag{12}$$

where $b_{\beta\alpha}(t) = -2\,Re\,(a_{\alpha\beta}^*\dot{\boldsymbol{R}}\cdot\boldsymbol{d}_{ij})$, $g_{\alpha\beta} = -g_{\beta\alpha}$, and $g_{\alpha\alpha} = 0$. The hopping probability $g_{\alpha\beta}$ is calculated at each nuclear integration timestep Δt and is evaluated stochastically by comparing to a random number $0 < \chi < 1$. The hop is performed if

$$\sum_{\gamma=1}^{\beta} g_{\alpha\gamma} < \chi < \sum_{\gamma=1}^{\beta+1} g_{\alpha\gamma} \tag{13}$$

where states are assumed to be ordered with increasing transition energy. If $\sum_{\gamma=1}^{N_S} g_{\alpha\gamma} < \chi < 1$ (where N_S is the number of states), then the system remains in state α. If $g_{\alpha\beta} < 0$, then the hop is unphysical and the probability is set to zero.[62] Finally, if a hop to a higher energy state is predicted, then there must be sufficient nuclear kinetic energy in the direction of NACR; otherwise, the hop is rejected (frustrated). After a successful hop, the total electron-nuclear energy is conserved by rescaling the nuclear velocity in the direction of the NACR according to the procedure described in refs 138, 139.

Here, we briefly describe several algorithmic improvements we implemented in NEXMD that reduce numerical cost, improve the accuracy of the FSSH algorithm, and allow numerical instability to be avoided.

Numerical Propagators. NACT and $c_i(t)$ are highly varying quantities that require evaluation at smaller quantum timesteps, δt, than standard nuclear timesteps, Δt (i.e., $\delta t < \Delta t$). The chosen value of δt must be small enough to resolve strongly localized peaks in NACT in order to avoid underestimating transition probabilities.[101] In NEXMD, eq 9 is solved numerically by separating the real and imaginary parts of $c_i(t)$ leading to coupled equations of motion described in detail in ref 100. The equations for the evolution of the quantum coefficients are solved at δt using the Runge−Kutta−Verner fifth- and sixth-order method[140,141] simultaneously with velocity Verlet propagation of eq 6 or 7 for the nuclei at Δt.

Importantly, the transition density matrices ξ_α may rarely change sign between two trajectory points ($\xi_\alpha(t) \sim -\xi_\alpha(t + \delta t)$) yielding incorrect NACR and NACT values computed according to eqs 10 and 11. In order to avoid the sign change, NEXMD tracks the relative phase of the transition density matrices at each timestep. Since $\xi_\alpha(t)$ and $\xi_\alpha(t + \delta t)$ are eigenvectors of eq 2, they obey the normalization condition $\langle\xi_\alpha \mid \xi_\beta\rangle = Tr(\rho_{00}[\xi_\alpha^\dagger\xi_\beta]) = \delta_{\alpha\beta}$, where $\delta_{\alpha\beta}$ is the Kronecker delta.

https://dx.doi.org/10.1021/acs.jctc.0c00248
J. Chem. Theory Comput. 2020, 16, 5771−5783

Therefore, if $\langle \xi_\alpha(t) \mid \xi_\alpha(t + \delta t)\rangle < 0$, then the sign of $\xi_\alpha(t + \delta t)$ is changed: $\xi_\alpha(t + \delta t) \rightarrow -\xi_\alpha(t + \delta t)$.

Trivial Unavoided Crossings. During NAMD simulations, it is important to treat trivial unavoided crossings (i.e., special cases of unavoided crossings[142]) that occur between two noninteracting states occupying the same energy range. For example, in extended polyatomic molecules composed of weakly coupled chromophores, these states are often spatially localized on separated chromophore units. At such crossing points, NACT becomes infinite and, within the FSSH algorithm, should produce a hop. However, the use of finite timestep numerical propagators for nuclear motion can cause such crossing points to be missed, causing adiabatic states to be misidentified, leading to artifacts in adiabatic state populations.[76,77] To overcome this technical challenge, we implemented a Min-Cost algorithm guiding the reassignment of the adiabatic states at the current timestep in terms of old states at the previous timestep.[76] The trivial crossing routine is a default NAMD procedure applied for all neighboring pairs of states. Finally, there are other algorithms that have been successfully applied to deal with the trivial crossing problem reported in refs 143−147 including some that were tested in the development NEXMD version.[148]

Decoherence Corrections. Introducing decoherence correction schemes[149−155] into surface hopping algorithms such as FSSH is critical[148] since the classical treatment of nuclei prohibits any dissipation of electronic coherence.[156] Moreover, the lack of such algorithms produces an internal inconsistency at the ensemble level manifested as the disagreement between the fraction of classical trajectories evolving on a given state $\frac{N_i(t)}{M}$ and the ensemble average quantum population for that state $\langle |c_i(t)|^2\rangle$. NEXMD implements an instantaneous decoherence approach[75] by reinitializing the quantum amplitude of the current state after every attempted hop (including forbidden hops). This provides qualitative improvement in the agreement between classical and quantum systems with no increase in computational cost.[75] Other empirical decoherence schemes implemented in NEXMD rely on the total kinetic energy or energy gaps.[157] These include methods such as the energy-based decoherence correction (EDC) and coherent switching with decay of mixing (CSDM) method.[158]

Computational Efficiency. In general, the computational efficiency of iterative algorithms is highly dependent on a good initial guess for the ground state (SCF procedure) and transition (Davidson algorithm) density matrices. Therefore, these quantities are stored from the previous trajectory point and reused as initial guesses in order to improve computational efficiency by nearly an order of magnitude. Notably, this may lead to a spurious energy drift particularly for NVE BOMD simulations. To offset this problem, the NEXMD implements an extended Lagrangian framework for excited state molecular dynamics.[159] Further, the propagation of electronic coefficients requires excited state energies $E_i(\boldsymbol{R})$ and NACTs to be evaluated at each quantum timestep. While this approach seems computationally expensive, linear interpolations take place only within each quantum timestep according to the requirements of the Runge−Kutta−Verner method. Therefore, the computational demand of obtaining $E_i(\boldsymbol{R})$ and NACTs at each quantum step can be offset by the use of a larger classical timestep without sacrificing precision in the quantum propagation. Larger classical timesteps reduce the computational cost in the calculation of the nuclear forces. Typically, values of 3−5 quantum steps combined with a classical timestep of 0.1−0.2 fs provide sufficient accuracy.[101] In addition, using analytical NACR and NACT allow these quantities to be computed separately, and the costly NACR is only computed at hopping instances to determine frustrated hops and for velocity rescaling.

CODE STRUCTURE AND WORKFLOW

Input and Output Files. For any type of calculation, there is a single NEXMD input file (input.ceon) containing all system specifications and parameters. The input file is read in two main namelists (&qmmm and &moldyn). Within the appropriate namespace, variable inputs can be set in any order, and the default values are assumed if left unspecified. The &qmmm namelist contains parameters largely used by the AMBER subroutines pertaining to geometry optimization, ground state and excited state calculations, convergence criteria, output options, solvent models, and external electric field. The &moldyn namelist is primarily utilized by NEXMD routines and contains parameters pertaining to molecular dynamics including nonadiabatic and thermostat specifications and output and log printing options. In addition, the nuclear coordinates [&coord: atom type (Z) and cartesian coordinates (x, y, z)] and velocities (&veloc: x, y, and z components corresponding to the atom order listed in coordinates) as well as the electronic state probabilities and phases (&coeff) must be specified in order to fully define the initial conditions of the system.

A detailed description of each output file generated by NEXMD for various functionalities is described in the manual. Here, we briefly touch on the more important NAMD-related files and under what conditions each is generated. In general, data is written to output files at user-specified intervals of the propagation timestep. Additionally, the verbosity tag in the input file controls the level of printing for the NAMD-related output. A summary of the additional output files generated at different verbosity levels for various types of NEXMD calculations is provided in Table S1 of the Supporting Information, and Table S2 lists the data printed in each output file at each verbosity level.

General Workflow and *getexcited.py* Package. We now turn our attention to the practical aspects of using the NEXMD code. Figure 1 schematically illustrates the general workflow for performing NAMD simulations. Here, each box represents a step in the workflow with connecting arrows to denote the direction. Above the arrows are the essential outputs passed between steps. First, the ground state of the system is determined and a ground state BOMD trajectory is run. From the thermally equilibrated ground state trajectory, geometries and their corresponding momenta are sampled to provide the initial conditions for the ensemble of NAMD (or BOMD) trajectories. For each configuration, a single-point calculation of energy and oscillator strengths is performed in order to produce an average optical spectrum. For each NAMD trajectory, the initial excited state is chosen based on the calculated excited state energies and oscillator strengths, and a different random seed is assigned. Note that the single-point calculations and optical spectrum steps can be bypassed if BOMD or NAMD is being performed starting from the same adiabatic state for each trajectory. Independent trajectories are then run in a trivially parallelizable fashion (1 processor = 1 trajectory) to save real time. Finally, post-processing of results is performed.

https://dx.doi.org/10.1021/acs.jctc.0c00248
J. Chem. Theory Comput. 2020, 16, 5771−5783

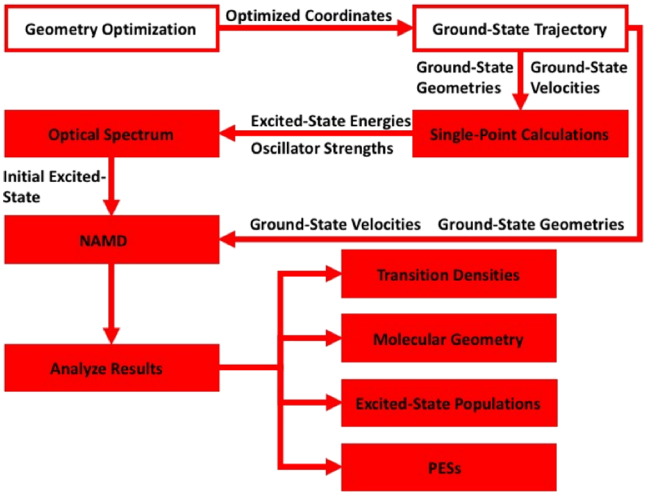

Figure 1. Schematic representation of the NAMD workflow using NEXMD. Filled red boxes indicate steps where the *getexcited.py* package can assist with generating input files for the swarm of trajectories and analysis. Arrows denote the direction of the workflow. Above the arrows are the required outputs from the previous step required for the next step.

In order to deal with the ensemble of trajectories, NEXMD includes the python package *getexcited.py*. The filled red boxes in Figure 1 indicate steps where the package can be used: automate the generation of input files for the swarm of trajectories by sampling initial configurations, calculating optical spectra, and populating the initial excitation and seed for the random number generator. Several standard analyses are also included in this package. The capabilities of this package are outlined in the following sections.

Sampling Initial Conditions. A swarm of excited state trajectories is propagated in the FSSH approach, each beginning from a different point in the phase space of initial coordinates and momenta. Sampling of initial conditions (snapshots of the molecular geometry $\boldsymbol{R}$ with their respective nuclear velocities $\dot{\boldsymbol{R}}$) is the first step in NAMD simulations. One common approach, employed in the *getexcited.py* package, is to sample the phase space from classical MD trajectories under the assumption that the system is in thermal equilibrium with its environment. Sampling the ground state conformational space should be adequate to represent the thermally equilibrated ensemble of molecules.[101] This requires computing a long (hundreds of ps) ground state BOMD trajectory using NVT propagation (eq 7) with parameters (temperature T and friction coefficient ζ) being consistent with future excited state simulations. Snapshots from the ground state BOMD trajectory give the initial postions and velocities for future excited state calculations. These snapshots are taken every 1−10 ps after the molecule has been equilibrated in the ground state for 10−50 ps, and an input file is generated for each configuration. The swarm of M trajectories provides a statistical average of results and is needed to perform population analysis and calculate relaxation rates, branching ratios, and quantum yields. The number of independent trajectories required to reach a statistical convergence can vary from system to system depending on the accessible conformational space. Several hundred trajectories are needed for realistic molecular materials.[101] Alternative procedures can be followed to achieve different conformational samplings but have not been implemented into our code release. For example, the Wigner distribution (quantum sampling)[160] requires calculation of vibrational normal modes and assumes that the molecule is at its zero-point energy level.

Optical Spectra. The next step is a single-point calculation for each configuration to generate excited state energies and transition dipole moments/oscillator strengths. These calculated values are used to produce an average optical spectrum (absorbance spectrum). The contribution to the total spectrum from each excited state α is modeled using either a Gaussian lineshape

$$A_\alpha(E) = f_{0\alpha}(E_\alpha)\frac{1}{\sigma\sqrt{2\pi}}\exp\left[-\frac{(E_\alpha - E)}{2\sigma^2}\right] \tag{14}$$

or a Lorentzian lineshape

$$A_\alpha(E) = f_{0\alpha}(E_\alpha)\frac{1}{\Gamma\pi}\frac{1}{1+\left[\frac{(E-E_\alpha)}{\Gamma}\right]^2} \tag{15}$$

Here, Γ and σ are spectral broadening related to the full width at half-maximum (FWHM) as FWHM $= 2\sqrt{2\ln 2}\,\sigma$ and FWHM $= 2\Gamma$. E_α and $f_{0\alpha}(E_\alpha)$ are the energy and oscillator strength of state α, respectively. The individual contributions are summed to obtain the total spectrum, which are then averaged over the M configurations.

Initial Excitation. Populating initial excited states requires the initial values of the quantum coefficients to be set according to a laser excitation wavelength, a laser pulse width, and excited state transition dipole moments/oscillator strengths. The total number of propagated excited states N_S should be large enough to include possible hops to the higher-energy states. All excited state trajectories are initialized in a pure state, i.e., $c_\alpha(t=0) = 1$ and $c_{\beta\neq\alpha}(t=0) = 0$, and all phase factors are initialized to zero. For each configuration, the probability of populating a given excited state α is calculated using a Gaussian-shaped Franck−Condon window centered at a specified energy, E_{FC}, according to

$$P_\alpha = f_{0\alpha}(E_\alpha)\frac{1}{\sigma\sqrt{2\pi}}\exp\left[-\frac{(E_\alpha - E_{FC})}{2\sigma^2}\right] \tag{16}$$

where σ defines the spectral broadening. The probabilities are normalized $P'_\alpha = P_\alpha/(\sum_{j=1}^{N_S} P_j)$ such that $\sum_{j=1}^{N_S} P'_j = 1$. A random number $0 < \chi \leq 1$ is generated, and state α is populated if

$$\sum_{j=1}^{\alpha} P'_{j-1} < \chi \leq \sum_{j=1}^{\alpha} P'_j \tag{17}$$

where $P'_0 = 0$ and adiabatic states are ordered with increasing energy. Due to thermal fluctuations and the stochastic determination of initial states in eq 17, the adiabatic state number for a given Franck−Condon window generally varies among all the configurations. In this step, the random seed for the number generator is also assigned. A different random seed must be assigned to each trajectory to avoid trajectory synchronization.[101,161]

PHOTOEXCITED DYNAMICS IN THE MODEL PPE DENDRIMER

In order to exemplify a typical simulation and analysis of results using NEXMD, we present the simulation of photoexcited dynamics in a model PPE dendrimer. The relevant input files for simulations presented in this section can be

https://dx.doi.org/10.1021/acs.jctc.0c00248
J. Chem. Theory Comput. 2020, 16, 5771−5783

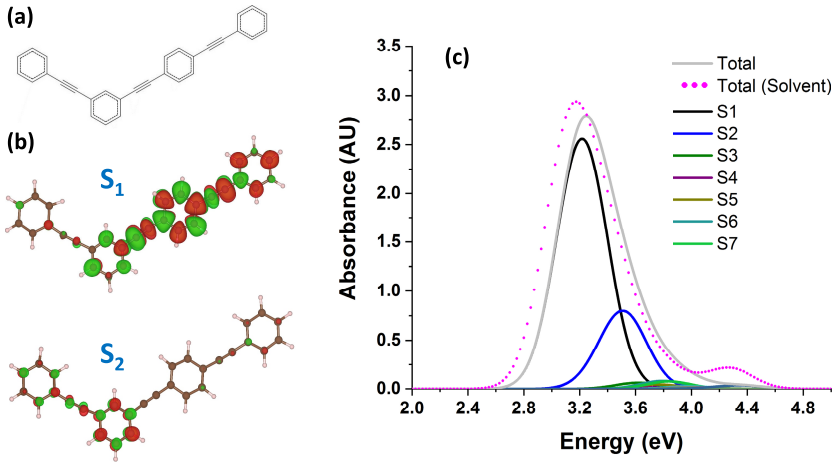

Figure 2. (a) Chemical structure of the model polyphenylene ehynylene (PPE) dendrimer composed of *meta*-linked 2-ring and 3-ring segments. (b) Orbital plot of the transition density for the S_1 and S_2 electronic states at the ground state optimized geometry. (c) Absorption spectrum of PPE at 300 K. Contributions from individual states are shown along with the total spectrum in vacuum (solid lines). The total absorption spectrum in solvent (ϵ = 30) is shown by the dotted line.

found in the Supporting Information. All of the analyses presented here are available in the *getexcited.py* package. The PPE dendrimer, whose chemical structure is displayed in Figure 2a, is composed of *meta*-substituted linear PPE segments of 2- and 3-rings (2,3-PPE). The analysis of the state transition densities at the optimized ground state configuration indicates that S_1 is localized mainly on the 3-ring segment (Figure 2b; top), whereas S_2 is localized mainly on the 2-ring segment (Figure 2b; bottom). Because of this energy gradient, it is expected that spatial energy transfer will occur from the 2-ring to the 3-ring segment following excitation to the higher energy S_2 state.[162]

Simulation Details. For all simulations presented here, the AM1/CIS level of theory has been used. We started by running a 1.3 ps ground-state MD trajectory of PPE in vacuum using Langevin propagation at 300 K with a timestep of 0.1 fs and friction coefficient of 20 ps^{-1}. From the equilibrated ground-state trajectory, 650 snapshots of nuclear geometries and velocities were sampled to provide initial conditions for excited state dynamics. The excited state dynamics were then investigated using BOMD in vacuum, NAMD in vacuum, and NAMD with solvent. For both BOMD and NAMD, all excited state trajectories were initialized in S_2 and propagated for 200 fs using Langevin dynamics (300 K, 20 ps^{-1}) with a classical timestep of 0.1 fs. For NAMD, a quantum timestep of 0.025 fs was used and 4 excited states were included in the simulations to allow for possible transitions to higher energy. The instantaneous decoherence correction was used, and trivial unavoided crossings were tracked by reducing the quantum timestep by a factor of 40. NAMD was also simulated in solvent using the same protocol as the vacuum NAMD simulations and applying the LR solvation model with the COSMO potential with a dielectric constant of 30, representing a polar solvent. Adiabatic simulations resulted in 501 trajectories that ran to completion, and NAMD simulations yielded 492 and 501 trajectories in vacuum and in solvent, respectively, that ran to completion.

Optical Spectra. The absorption spectrum of the branched PPE molecule in Figure 2a is calculated using the thermally equilibrated ground state conformational sampling at 300 K with a Gaussian lineshape and FWHM of 0.36 eV. The spectrum, shown in Figure 2c, includes the contributions of the 11 lowest-energy excited states. S_1 and S_2 are strongly absorbing with high oscillator strength, while higher-energy states are optically forbidden. The spectrum calculated in the presence of solvent is red-shifted by ~0.1 eV compared to its vacuum counterpart (solvatochromic shift).[85]

Analysis of Electronic Dynamics. During nonadiabatic dynamics, the overall relaxation from the initially excited electronic state (S_2) to the lowest-energy excited state (S_1) can be monitored by tracking the evolution of the adiabatic state populations. Populations can be calculated within a classical or quantum framework. The classical description of state populations in surface hopping simulations is calculated as the fraction of independent trajectories evolving on a given state at any time $\frac{N_i(t)}{M}$. State populations can also be calculated quantum-mechanically from the time-dependent adiabatic expansion coefficients to give the average quantum population $\langle |c_i(t)|^2 \rangle$. Figure 3 shows the classical and quantum adiabatic state populations during NAMD simulations of the PPE dendrimer in vacuum (panel a) and in solvent (panel b). The population analysis reveals that the population initially in S_2 decays while the population of the lowest-energy state S_1 rises on a sub-100 fs timesale. Higher-energy states S_3 and S_4 do not gain any significant population. Finally, it is important to note that the quantum populations (dotted lines) agree qualitatively with the classical fraction of trajectories (solid lines) due to the use of the instantaneous decoherence correction. In order to understand the difference in relaxation rates in vacuum and solvent, the PES and energy gaps during NAMD can be further investigated.[85]

Finally, the spatial energy transfer can be monitored by following the time-dependent localization of the electronic transition density $\rho_{0\alpha}$ (eq 1). The orbital representation of the diagonal elements $(\rho_{0\alpha})_{nn}$ in AO basis functions n provides a convenient measure of the spatial location of the excited state wave function. By partitioning the molecule into moieties and/or chromophore units, the fraction of transition density, $(\rho^{0\alpha}(t))^2_X$, localized on each unit X at any given time is calculated by summing the contributions of the AOs from each atom (index A) in X and half the contribution of the AOs from atoms localized on the boundary with another unit (index B), as printed in the output file transition-densities.out.

https://dx.doi.org/10.1021/acs.jctc.0c00248
J. Chem. Theory Comput. 2020, 16, 5771−5783

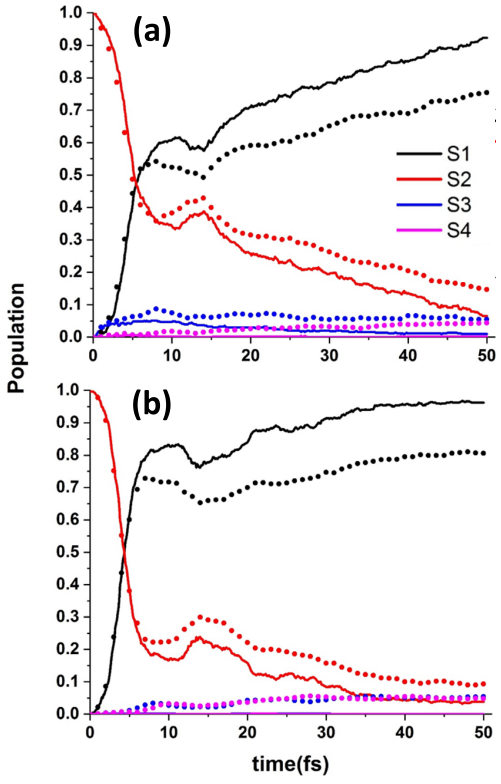

Figure 3. Evolution of adiabatic state populations during NAMD simulations of the PPE dendrimer in (a) vacuum and (b) solvent (ϵ = 30). Both the classical fraction of trajectories (solid lines) and the quantum populations (dotted lines) are plotted for the 4 lowest-energy excited states.

$$(\rho^{0\alpha}(t))_X^2 = \sum_{n_A m_A} (\rho^{0\alpha}_{n_A m_A}(t))^2 + \frac{1}{2} \sum_{n_B m_B} (\rho^{0\alpha}_{n_B m_B}(t))^2 \quad (18)$$

The evolution of the transition density localization is illustrated in Figure 4. First, the PPE dendrimer is divided into subunits TD1 and TD2 (Figure 4a). These correspond to the 3-ring and 2-ring segments where the transition densities of S_1 and S_2 are primarily localized, respectively (see Figure 2). The initial excitation corresponds to S_2 in both BOMD and NAMD simulations. Because the S_2 state can be localized on the 2- or 3-ring unit due to conformational variations (as discussed above), the initial transition density localizations are 65% in TD2 (2-ring) and 35% in TD1 (3-ring).

During BOMD simulations (Figure 4b), an initial distribution of transition density is maintained on each unit throughout the dynamics with no energy transfer between them. Oscillations in localization during adiabatic dynamics on S_2 arise from changes in the molecular configurations that can cause variations in the localization of excitations. In contrast, during NAMD simulations (Figure 4c), the initial excitation primarily localized in TD2 undergoes energy transfer to TD1. The fraction of transition density localized in TD2 decays, while the fraction of transition density in TD1 increases to almost 80% after 50 fs. Such spatial energy transfer is concomitant to population transfer (Figure 3), and, like the population transfer, is faster in solvent.

CONCLUSIONS

We present the functionalities of the NEXMD, a versatile software package for modeling ground and excited state

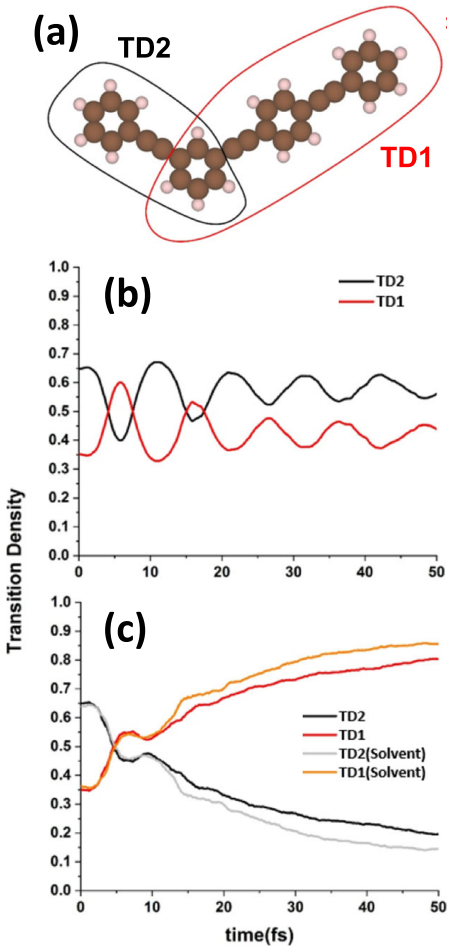

Figure 4. (a) Division of the PPE dendrimer into subunits TD1 and TD2 used for transition density analysis. (b) The evolution of the fraction of transition density localized in each unit during adiabatic BOMD. (c) The evolution of the fraction of transition density localized in each unit during NAMD simulations in vacuum and solvent.

molecular dynamics. NEXMD is capable of geometry optimizations and simulating both the Born–Oppenheimer and nonadiabatic molecular dynamics. The latter is powered by the FSSH algorithm that is able to model quantum transitions between excited states and nonradiative electron–phonon relaxation (internal conversion). The RPA (or CIS) framework for excited state calculations coupled with semiempirical model Hamiltonians (AM1, PM3, PM6, etc.) allows for efficient simulations of NAMD on several picosecond timescales in large molecular systems with hundreds of atoms and tens of excited states using the native excited state PES. This electronic structure approach provides reasonably accurate ground state geometries and energies, heats of formation, vertical excitation energies, polarizabilities, and adiabatic excited state PESs. Numerical efficiency is also attributed to analytic calculation of excited state gradients and nonadiabatic couplings, as well as many other numerical algorithm improvements. Our NAMD implementation goes beyond the standard FSSH recipes by including identification for trivial unavoided crossings and the decoherence correction schemes. Along with dynamics, a wealth of molecular metrics is available (either during dynamics or as single-point calculations) including oscillator strengths, various dipole moments,

https://dx.doi.org/10.1021/acs.jctc.0c00248
J. Chem. Theory Comput. 2020, 16, 5771−5783

Mulliken charges, and transition densities. The more realistic description of the molecular system can be achieved when using implicit solvation models (LR, SS, VE) using COSMO approach.

We extensively illustrated the methodology and algorithms employed in the currently released NEXMD software and *getexcited.py* package. To demonstrate these capabilities, we presented a case study of the photoexcited dynamics of the model PPE dendrimer, which exhibits energy transfer during the NAMD simulations following excitation of higher-lying excited states. Several of the analysis features available in the *getexcited.py* package (such as calculations of spectra, nonradiative relaxation rates, and transition density evolution) are illustrated. There are many other types of analyses available such as vibrational modes, variations of molecular conformations (bond length alternations and dihedral angles), transition density matrices, etc.

It is important to note that many other approaches have been developed over the years for modeling excited states and their dynamics. We have not gone into details of these other methods in this paper nor do we suggest that the approaches currently implemented in NEXMD are preferable over other methods. For a more detailed description of various NAMD and surface hopping methods, we refer the reader to our recent review.[148] We invite the community to implement any method of their choice into the NEXMD program or to develop any analysis of their choice by creating a new module for the python-based *getexcited.py* package. For example, we have recently implemented in the development version of NEXMD a more accurate NAMD framework, namely, multiconfigurational Ehrenfest ab initio multiple cloning.[52,163] We hope NEXMD will further grow into a versatile, powerful, and user-friendly software package that will prove useful for a large array of chemical applications.

■ ASSOCIATED CONTENT

Supporting Information

The Supporting Information is available free of charge at https://pubs.acs.org/doi/10.1021/acs.jctc.0c00248.

> Table of NEXMD output files generated at different verbosity levels for each functionality. Table of data written to output files for different verbosity levels. Example NEXMD input files for ground state dynamics, single-point calculations, adiabatic excited state dynamics, nonadiabatic excited-state dynamics in vacuum, and nonadiabatic excited state dynamics in a solvent (ZIP)

■ AUTHOR INFORMATION

Corresponding Authors

Tammie R. Nelson − *Physics and Chemistry of Materials, Theoretical Division and Center for Integrated Nanotechnologies, Los Alamos National Laboratory, Los Alamos, New Mexico 87545, United States;* orcid.org/0000-0002-3173-5291; Email: tammien@lanl.gov

Sergei Tretiak − *Physics and Chemistry of Materials, Theoretical Division, Los Alamos National Laboratory, Los Alamos, New Mexico 87545, United States;* orcid.org/0000-0001-5547-3647; Email: serg@lanl.gov

Authors

Walter Malone − *Physics and Chemistry of Materials, Theoretical Division and Center for Nonlinear Studies, Los Alamos National Laboratory, Los Alamos, New Mexico 87545, United States;* orcid.org/0000-0001-8245-322X

Benjamin Nebgen − *Physics and Chemistry of Materials, Theoretical Division, Los Alamos National Laboratory, Los Alamos, New Mexico 87545, United States*

Alexander White − *Physics and Chemistry of Materials, Theoretical Division, Los Alamos National Laboratory, Los Alamos, New Mexico 87545, United States*

Yu Zhang − *Physics and Chemistry of Materials, Theoretical Division, Los Alamos National Laboratory, Los Alamos, New Mexico 87545, United States;* orcid.org/0000-0001-8938-1927

Huajing Song − *Physics and Chemistry of Materials, Theoretical Division, Los Alamos National Laboratory, Los Alamos, New Mexico 87545, United States;* orcid.org/0000-0001-5958-7377

Josiah A. Bjorgaard − *Physics and Chemistry of Materials, Theoretical Division, Los Alamos National Laboratory, Los Alamos, New Mexico 87545, United States;* orcid.org/0000-0003-3679-2487

Andrew E. Sifain − *U.S. Army Research Laboratory, Aberdeen, Maryland 21005, United States;* orcid.org/0000-0002-2964-1923

Beatriz Rodriguez-Hernandez − *Universidad Nacional de Quilmes/CONICET, B1876BXD Bernal, Argentina*

Victor M. Freixas − *Universidad Nacional de Quilmes/CONICET, B1876BXD Bernal, Argentina;* orcid.org/0000-0003-1733-4827

Sebastian Fernandez-Alberti − *Universidad Nacional de Quilmes/CONICET, B1876BXD Bernal, Argentina;* orcid.org/0000-0002-0916-5069

Adrian E. Roitberg − *Department of Chemistry, University of Florida, Gainesville, Florida 32611, United States;* orcid.org/0000-0003-3963-8784

Complete contact information is available at: https://pubs.acs.org/10.1021/acs.jctc.0c00248

Notes

The authors declare no competing financial interest.

Program code, license, and documentation may be accessed at https://github.com/lanl/NEXMD.

■ ACKNOWLEDGMENTS

The work at Los Alamos National Laboratory (LANL) was supported by the LANL Directed Research and Development Funds (LDRD) and performed in part at the Center for Nonlinear Studies (CNLS) and the Center for Integrated Nanotechnologies (CINT), a U.S. Department of Energy, Office of Science User Facility at LANL. This research used resources provided by the LANL Institutional Computing (IC) Program. LANL is operated by Triad National Security, LLC, for the National Nuclear Security Administration of the U.S. Department of Energy (Contract No. 89233218NCA000001). S.F.-A., A.E.R., and B.R.-H. also acknowledge CONICET, UNQ, ANPCyT (PICT-2018-02360) for their support. This work has been developed in part within the Umbrella non proprietary user agreement involving Los Alamos National Laboratory, Sandia National Laboratories and Universidad Nacional de Quilmes.

REFERENCES

(1) Salehi, A.; Fu, X.; Shin, D.-H.; So, F. Recent Advances in OLED Optical Design. *Adv. Func. Mater.* **2019**, *29*, 1808803.

(2) Bredas, J.-L.; Norton, J. E.; Cornil, J.; Coropceanu, V. Molecular understanding of organic solar cells: The challenges. *Acc. Chem. Res.* **2009**, *42*, 1691−1699.

(3) Wang, N.; Tong, X.; Burlingame, Q.; Yu, J.; Forrest, S. R. Photodegradation of small-molecule organic photovoltaics. *Sol. Energy Mater. Sol. Cells* **2014**, *125*, 170−175.

(4) Wolfer, P.; Armin, A.; Pivrikas, A.; Velusamy, M.; Burn, P. L.; Meredith, P. Solution Structure: Defining Polymer Film Morphology and Optoelectronic Device Performance. *J. Mater. Chem. C* **2014**, *2*, 71−77.

(5) Schmidt-Hansberg, B.; Sanyal, M.; Klein, M. F. G.; Pfaff, M.; Schnabel, N.; Jaiser, S.; Vorobiev, A.; Muller, E.; Colsmann, A.; Scharfer, P.; Gerthsen, D.; Lemmer, U.; Barrena, E.; Schabel, W. Moving Through the Phase Diagram: Morphology Formation in Solution Cast Polymer-Fullerene Blend Films for Organic Solar Cells. *ACS Nano* **2011**, *5*, 8579−8590.

(6) Zhugayevych, A.; Tretiak, S. Theoretical Description of Structural and Electronic Properties of Organic Photovoltaic Materials. *Annu. Rev. Phys. Chem.* **2015**, *66*, 305.

(7) Sirringhaus, H.; Kawase, T.; Friend, R. H.; Shimoda, T.; Inbasekaran, M.; Wu, W.; Woo, E. P. High-resolution inkjet printing of all-polymer transistor circuits. *Science* **2000**, *290*, 2123−2126.

(8) Lee, K. E.; Lee, J. U.; Seong, D. G.; Um, M.-K.; Lee, W. Highly Sensitive Ultraviolet Light Sensor Based on Photoactive Organic Gate Dielectrics with an Azobenzene Derivative. *J. Phys. Chem. C* **2016**, *120*, 23172−23179.

(9) Satishkumar, B. C.; Brown, L. O.; Gao, Y.; Wang, C.-C.; Wang, H.-L.; Doorn, S. K. Reversible fluorescence quenching in carbon nanotubes for biomolecular sensing. *Nat. Nanotechnol.* **2007**, *2*, 560−564.

(10) Maksimov, E. G.; Yaroshevich, I. A.; Tsoraev, G. V.; Sluchanko, N. N.; Slutskaya, E. A.; Shamborant, O. G.; Bobik, T. V.; Friedrich, T.; Stepanov, A. V. A genetically encoded fluorescent temperature sensor derived from the photoactive Orange Carotenoid Protein. *Sci. Rep.* **2019**, *9*, 8937.

(11) Li, H.; Wang, J.; Wang, X.; Lin, H.; Li, F. Perylene-Based Photoactive Material as a Double-Stranded DNA Intercalating Probe for Ultrasensitive Photoelectrochemical Biosensing. *ACS Appl. Mater. Interfaces* **2019**, *11*, 16958−16964.

(12) Wilson, A.; Punginelli, C.; Gall, A.; Bonetti, C.; Alexandre, M.; Routaboul, J.-M.; Kerfeld, C. A.; van Grondelle, R.; Robert, B.; Kennis, J. T. M.; Kirilovsky, D. A photoactive carotenoid protein acting as light intensity sensor. *Proc. Nat. Acad. Sci.* **2008**, *105*, 12075−12080.

(13) Romero, N. A.; Nicewicz, D. A. Organic Photoredox Catalysis. *Chem. Rev.* **2016**, *116*, 10075−10166.

(14) Granström, M.; Petritsch, K.; Arias, A. C.; Lux, A.; Andersson, M. R.; Friend, R. H. Laminated fabrication of polymeric photovoltaic diodes. *Nature* **1998**, *395*, 257−260.

(15) Cao, Y.; Parker, I. D.; Yu, G.; Zhang, C.; Heeger, A. J. Improved quantum efficiency for electroluminescence in semiconducting polymers. *Nature* **1999**, *397*, 414−417.

(16) Friend, R. H.; Gymer, R. W.; Holmes, A. B.; Burroughes, J. H.; Marks, R. N.; Taliani, C.; Bradley, D. D. C.; Dos Santos, D. A.; Brédas, J. L.; Lögdlund, M.; Salaneck, W. R. Electroluminescence in conjugated polymers. *Nature* **1999**, *397*, 121−128.

(17) Tretiak, S.; Saxena, A.; Martin, R. L.; Bishop, A. R. Conformational dynamics of photoexcited conjugated molecules. *Phys. Rev. Lett.* **2002**, *89*, No. 097402.

(18) Bricker, W. P.; Shenai, P. M.; Ghosh, A.; Liu, Z.; Enriquez, M. G. M.; Lambrev, P. H.; Tan, H.-S.; Lo, S. T.; Fernandez-Alberti, S.; Zhao, Y. Non-radiative Relaxation of Photoexcited Chlorophylls: Theoretical and Experimental Study. *Sci. Rep.* **2015**, *5*, 13625.

(19) Shenai, P. M.; Fernandez-Alberti, S.; Bricker, W. P.; Tretiak, S.; Zhao, Y. Internal Conversion and Vibrational Energy Redistribution in Chlorophyll A. *J. Phys. Chem. B* **2016**, *120*, 49−58.

(20) Polli, D.; Altoé, P.; Weingart, O.; Spillane, K. M.; Manzoni, C.; Brida, D.; Tomasello, G.; Orlandi, G.; Kukura, P.; Mathies, R. A.; Garavelli, M.; Cerullo, G. Conical intersection dynamics of the primary photoisomerization event in vision. *Nature* **2010**, *467*, 440−443.

(21) Ostroumov, E. E.; Mulvaney, R. M.; Cogdell, R. J.; Scholes, G. D. Broadband 2D Electronic Spectroscopy Reveals a Carotenoid Dark State in Purple Bacteria. *Science* **2013**, *340*, 52−56.

(22) Scholes, G. D.; et al. Using Coherence to Enhance Function in Chemical and Biophysical Systems. *Nature* **2017**, *543*, 647−656.

(23) Huix-Rotllant, M.; Tamura, H.; Burghardt, I. Concurrent Effects of Delocalization and Internal Conversion Tune Charge Separation at Regioregular Polythiophene-Fullerene Heterojunctions. *J. Phys. Chem. Lett.* **2015**, *6*, 1702−1708.

(24) Brédas, J.-L.; Beljonne, D.; Coropceanu, V.; Cornil, J. Charge-Transfer and EnergyTransfer Processes in π-Conjugated Oligomers and Polymers: A Molecular Picture. *Chem. Rev.* **2004**, *104*, 4971−5004.

(25) Lin, H.-C.; Jin, B.-Y. Charge-Transfer Interactions in Organic Functional Materials. *Materials* **2010**, *3*, 4214−4251.

(26) Osuka, A.; Fujikane, D.; Shinmori, H.; Kobatake, S.; Irie, M. Synthesis and Photoisomerization of Dithienylethene-Bridged Diporphyrins. *J. Org. Chem.* **2001**, *66*, 3913−3923.

(27) Suda, M.; Thathong, Y.; Promarak, V.; Kojima, H.; Nakamura, M.; Shiraogawa, T.; Ehara, M.; Yamamoto, H. M. Light-driven molecular switch for reconfigurable spin filters. *Nature Comm.* **2019**, *10*, 2455.

(28) George, C.; Ammann, M.; D'Anna, B.; Donaldson, D. J.; Nizkorodov, S. A. Heterogeneous Photochemistry in the Atmosphere. *Chem. Rev.* **2015**, *115*, 4218−4258.

(29) Grannas, A. M.; Pagano, L. P.; Pierce, B. C.; Bobby, R.; Fede, A. Role of Dissolved Organic Matter in Ice Photochemistry. *Environ. Sci. Technol.* **2014**, *48*, 10725−10733.

(30) Barbatti, M.; Aquino, A. J. A.; Szymczak, J. J.; Nachtigallova, D.; Hobza, P.; Lischka, H. Relaxation mechanisms of UV-photoexcited DNA and RNA nucleobases. *Proc. Natl. Acad. Sci. U. S. A.* **2010**, *107*, 21453−21458.

(31) Groenhof, G.; Bouxin-Cademartory, M.; Hess, B.; de Visser, S. P.; Berendsen, H. J. C.; Olivucci, M.; Mark, A. E.; Robb, M. A. Photoactivation of the Photoactive Yellow Protein: Why Photon Absorption Triggers a Trans-to-Cis Isomerization of the Chromophore in the Protein. *J. Am. Chem. Soc.* **2004**, *126*, 4228−4233.

(32) Barbatti, M.; Ruckenbauer, M.; Plasser, F.; Pittner, J.; Granucci, G.; Persico, M.; Lischka, H. Newton-X: a surface-hopping program for nonadiabatic molecular dynamics. *WIREs Comput. Mol. Sci.* **2014**, *4*, 26−33.

(33) Akimov, A. V.; Prezhdo, O. V. The PYXAID Program for Non-Adiabatic Molecular Dynamics in Condensed Matter Systems. *J. Chem. Theory Comput.* **2013**, *9*, 4959−4972.

(34) Akimov, A. V.; Prezhdo, O. V. Advanced Capabilities of the PYXAID Program: Integration Schemes, Decoherence Effects, Multiexcitonic States, and Field-Matter Interaction. *J. Chem. Theory Comput.* **2014**, *10*, 789−804.

(35) Valiev, M.; Bylaska, E. J.; Govind, N.; Kowalski, K.; Straatsma, T. P.; Van Dam, H. J. J.; Wang, D.; Nieplocha, J.; Apra, E.; Windus, T. L.; de Jong, W. A. NWChem: A Comprehensive and Scalable Open-Source Solution for Large Scale Molecular Simulations. *Comput. Phy. Commun.* **2010**, *181*, 1477−1489.

(36) Shao, Y.; et al. Advances in molecular quantum chemistry contained in the Q-Chem 4 program package. *Mol. Phys.* **2015**, *113*, 184−215.

(37) Richter, M.; Marquetand, P.; González-Vázquez, J.; Sola, I.; González, L. SHARC: *ab Initio* Molecular Dynamics with Surface Hopping in the Adiabatic Representation Including Arbitrary Couplings. *J. Chem. Theory Comput.* **2011**, *7*, 1253−1258.

(38) Mai, S.; Marquetand, P.; González, L. Nonadiabatic Dynamics: The Sharc Approach. *WIREs Comput. Mol. Sci.* **2018**, *8*, No. e1370.

(39) Weingart, O.; Nenov, A.; Altoè, P.; Rivalta, I.; Segarra-Martí, J.; Dokukina, I.; Garavelli, M. COBRAMM 2.0—A software interface for

https://dx.doi.org/10.1021/acs.jctc.0c00248
J. Chem. Theory Comput. 2020, 16, 5771−5783

tailoring molecular electronic structure calculations and running nanoscale (QM/MM) simulations. *J. Mol. Model.* **2018**, *24*, 271.
(40) Niklasson, A. M. N.; Steneteg, P.; Odell, A.; Bock, N.; Challacombe, M.; Tymczak, C. J.; Holmstrom, E.; Zheng, G.; Weber, V. Extended Langevin Born-Oppenheimer molecular dynamics with dissipation. *J. Chem. Phys.* **2009**, *130*, 214109.
(41) Karabunarliev, S.; Baumgarten, M.; Müllen, K. Adiabatic one- and two-photon excited states in phenylene-based conjugated oligomers: A quantum-chemical study. *J. Phys. Chem. A* **2000**, *104*, 8236−8243.
(42) Molnar, F.; Ben-Nun, M.; Martínez, T. J.; Schulten, K. Characterization of conical intersections between the ground and first excited state for a retinal analog. *J. Mol. Struct. Theochem.* **2000**, *506*, 169−178.
(43) Franco, I.; Tretiak, S. Electron-vibrational dynamics of photoexcited polyfluorenes. *J. Am. Chem. Soc.* **2004**, *126*, 12130−12140.
(44) Gambetta, A.; Manzoni, C.; Menna, E.; Meneghetti, M.; Cerullo, G.; Lanzani, G.; Tretiak, S.; Piryatinski, A.; Saxena, A.; Martin, R. L.; Bishop, A. R. Real-time observation of nonlinear coherent phonon dynamics in single-walled carbon nanotubes. *Nat. Phys.* **2006**, *2*, 515−520.
(45) Jasper, A. W.; Nangia, S.; Zhu, C.; Truhlar, D. G. Non-Born-Oppenheimer molecular dynamics. *Acc. Chem. Res.* **2006**, *39*, 101−108.
(46) Baer, M. *Beyond Born-Oppenheimer. Electronic Nonadiabatic Coupling Terms and Conical Intersections*; Wiley-Interscience, A John Wiley & Son, Inc.: Hoboken, New Jersey, 2006.
(47) Beck, M. H.; Jäckle, A.; Worth, G. A.; Meyer, H.-D. The multiconfiguration timedependent Hartree (MCTDH) method: a highly efficient algorithm for propagating wavepackets. *Phys. Reports* **2000**, *324*, 33.
(48) Yeager, D. L.; Jørgensen, P. A multiconfigurational time-dependent hartree-fock approach. *Chem. Phys. Lett.* **1979**, *65*, 77.
(49) Stock, G.; Thoss, M. Semiclassical Description of Nonadiabatic Quantum Dynamics. *Phys. Rev. Lett.* **1997**, *78*, 578.
(50) Curchod, B. F. E.; Martinez, T. J. Ab Initio Nonadiabatic Quantum Molecular Dynamics. *Chem. Rev.* **2018**, *118*, 3305.
(51) Ben-Nun, M.; Quenneville, J.; Mártinez, T. J. Ab Initio Multiple Spawning: Photochemistry from First Principles Quantum Molecular Dynamics. *J. Phys. Chem. A* **2000**, *104*, 5161.
(52) Makhov, D. V.; Symonds, C.; Fernandez-Alberti, S.; Shalashilin, D. V. *Ab initio* quantum direct dynamics simulations of ultrafast photochemistry with Multiconfigurational Ehrenfest approach. *Chem. Phys.* **2017**, *493*, 200.
(53) Miller, W. H. Electronically Nonadiabatic Dynamics via Semiclassical Initial Value Methods. *J. Phys. Chem. A* **2009**, *113*, 1405−1415.
(54) Herman, M. F. Toward an Accurate and Efficient Semiclassical Surface Hopping Procedure for Nonadiabatic Problems. *J. Phys. Chem. A* **2005**, *109*, 9196−9205.
(55) Kong, X.; Markmann, A.; Batista, V. S. Time-Sliced Thawed Gaussian Propagation Method for Simulations of Quantum Dynamics. *J. Phys. Chem. A* **2016**, *120*, 3260−3269.
(56) White, A. J.; Gorshkov, V. N.; Wang, R.; Tretiak, S.; Mozyrsky, D. Semiclassical Monte Carlo: A First Principles Approach to Non-Adiabatic Molecular Dynamics. *J. Chem. Phys.* **2014**, *141*, 184101.
(57) Curchod, B. F. E.; Rauer, C.; Marquetand, P.; González, L.; Martinez, T. J. Communication: GAIMS—Generalized *Ab Initio* Multiple Spawning for Both Internal Conversion and Intersystem Crossing Processes. *J. Chem. Phys.* **2016**, *144*, 101102.
(58) Crespo-Otero, R.; Barbatti, M. Recent Advances and Perspectives on Nonadiabatic Mixed Quantum-Classical Dynamics. *Chem. Rev.* **2018**, *118*, 7026.
(59) Kapral, R. Progress in the theory of mixed quantum-classical dynamics. *Annu. Rev. Phys. Chem.* **2006**, *57*, 129.
(60) Wang, L.; Akimov, A.; Prezhdo, O. V. Recent Progress in Surface Hopping: 2011-2015. *J. Phys. Chem. Lett.* **2016**, *7*, 2100.
(61) Tully, J. C. Mixed Quantum Classical Dynamics. *Faraday Discuss.* **1998**, *110*, 407−419.
(62) Tully, J. C. Molecular Dynamics with Electronic Transitions. *J. Chem. Phys.* **1990**, *93*, 1061−1071.
(63) Case, D. *AMBER 2018*; University of California: San Francisco, 2018.
(64) Jorgensen, P. Molecular and Atomic Applications of Time-Dependent Hartree-Fock Theory. *Annu. Rev. Phys. Chem.* **1975**, *26*, 359.
(65) Yarkony, D. R. *Modern Electronic Structure Theory*; World Scientific Publishing Company: 1995.
(66) McLachlan, A. D.; Ball, M. A. Time-Dependent Hartree-Fock Theory for Molecules. *Rev. Mod. Phys.* **1964**, *36*, 844.
(67) Thouless, D. J. *The Quantum Mechanics of Many-Body Systems*; Academic Press: New York, 1972.
(68) Chernyak, V.; Mukamel, S. Density-matrix representation of nonadiabatic couplings in time-dependent density functional (TDDFT) theories. *J. Chem. Phys.* **2000**, *112*, 3572−3579.
(69) Tommasini, M.; Chernyak, V.; Mukamel, S. Electronic Density-Matrix Algorithm for Nonadiabatic Couplings in Molecular Dynamics Simulations. *Int. J. Quantum Chem.* **2001**, *85*, 225−238.
(70) Furche, F. On the density matrix based approach to time-dependent density functional response theory. *J. Chem. Phys.* **2001**, *114*, 5982−5992.
(71) Furche, F.; Ahlrichs, R. Adiabatic Time-Dependent Density Functional Methods for Excited State Properties. *J. Chem. Phys.* **2002**, *117*, 7433−7447.
(72) Tretiak, S.; Chernyak, V. Resonant nonlinear polarizabilities in the time-dependent functional theory. *J. Chem. Phys.* **2003**, *119*, 8809−8823.
(73) Akimov, A. V.; Neukirch, A. J.; Prezhdo, O. V. Theoretical Insights into Photoinduced Charge Transfer and Catalysis at Oxide Interfaces. *Chem. Rev.* **2013**, *113*, 4496−4565.
(74) Cramer, C. J.; Truhlar, D. G. Implicit Solvation Models: Equilibria, Structure, Spectra, and Dynamics. *Chem. Rev.* **1999**, *99*, 2161−2200.
(75) Nelson, T.; Fernandez-Alberti, S.; Roitberg, A. E.; Tretaik, S. Nonadiabatic ExcitedState Molecular Dynamics: Treatment of Electronic Decoherence. *J. Chem. Phys.* **2013**, *138*, 224111.
(76) Fernandez-Alberti, S.; Roitberg, A.; Nelson, T.; Tretiak, S. Identification of Unavoided Crossings in Nonadiabatic Photoexcited Dynamics Involving Multiple Electronic States in Polyatomic Conjugated Molecules. *J. Chem. Phys.* **2012**, *137*, No. 014512.
(77) Nelson, T.; Fernandez-Alberti, S.; Roitberg, A. E.; Tretiak, S. Artifacts Due to Trivial Unavoided Crossings in the Modeling of Photoinduced Energy Transfer Dynamics in Extended Conjugated Molecules. *Chem. Phys. Lett.* **2013**, *590*, 208−213.
(78) Clark, J.; Nelson, T.; Tretiak, S.; Cirmi, G.; Lanzani, G. Femtosecond Torsional Relaxation. *Nat. Phys.* **2012**, *8*, 225−231.
(79) Oldani, N.; Tretiak, S.; Bazan, G.; Fernandez-Alberti, S. Modeling of internal conversion in photoexcited conjugated molecular donors used in organic photovoltaics. *Energy Environ. Sci.* **2014**, *7*, 1175−1184.
(80) Ondarse-Alvarez, D.; Oldani, N.; Tretiak, S.; Fernandez-Alberti, S. Computational study of photoexcited dynamics in bichromophoric cross-shaped oligofluorene. *J. Phys. Chem. A* **2014**, *118*, 10742−10753.
(81) Alfonso Hernandez, L.; Nelson, T.; Gelin, M. F.; Lupton, J. M.; Tretiak, S.; Fernandez-Alberti, S. Interference of Interchromophoric Energy-Transfer Pathways in π-Conjugated Macrocycles. *J. Phys. Chem. Lett.* **2016**, *7*, 4936−4944.
(82) Franklin-Mergarejo, R.; Nelson, T.; Tretiak, S.; Fernandez-Alberti, S. Phonon bottleneck and long-lived excited states in π-conjugated pyrene hoop. *Phys. Chem. Chem. Phys.* **2017**, *19*, 9478−9484.
(83) Oldani, N.; Doorn, S. K.; Tretiak, S.; Fernandez-Alberti, S. Photoinduced dynamics in cycloparaphenylenes: planarization, electron-phonon coupling, localization and intraring migration of

https://dx.doi.org/10.1021/acs.jctc.0c00248
J. Chem. Theory Comput. 2020, 16, 5771−5783

the electronic excitation. *Phys. Chem. Chem. Phys.* **2017**, *19*, 30914−30924.
(84) Athanasopoulos, S.; Hernandez, L. A.; Beljonne, D.; Fernandez-Alberti, S.; Tretiak, S. Ultrafast Non-Förster Intramolecular Donor-Acceptor Excitation Energy Transfer. *J. Phys. Chem. Lett.* **2017**, *8*, 1688−1694.
(85) Sifain, A. E.; Bjorgaard, J. A.; Nelson, T. R.; Nebgen, B. T.; White, A. J.; Gifford, B. J.; Gao, D. W.; Prezhdo, O. V.; Fernandez-Alberti, S.; Roitberg, A. E.; Tretiak, S. Photoexcited Nonadiabatic Dynamics of Solvated Push-Pull π-Conjugated Oligomers with the NEXMD Software. *J. Chem. Theory Comput.* **2018**, *14*, 3955−3966.
(86) Rodriguez-Hernández, B.; Ondarse-Álvarez, D.; Oldani, N.; Martinez-Mesa, A.; Uranga-Piña, L.; Tretiak, S.; Fernández-Alberti, S. Modification of Optical Properties and Excited-State Dynamics by Linearizing Cyclic Paraphenylene Chromophores. *J. Phys. Chem. C* **2018**, *122*, 16639−16648.
(87) Ondarse-Alvarez, D.; Nelson, T.; Lupton, J. M.; Tretiak, S.; Fernandez-Alberti, S. Let Digons be Bygones: The Fate of Excitons in Curved π-Systems. *J. Phys. Chem. Lett.* **2018**, *9*, 7123−7129.
(88) Franklin-Mergarejo, R.; Alvarez, D. O.; Tretiak, S.; Fernandez-Alberti, S. Carbon nanorings with inserted acenes: breaking symmetry in excited state dynamics. *Sci. Rep.* **2016**, *6*, 31253.
(89) Hernandez, L. A.; Nelson, T.; Tretiak, S.; Fernandez-Alberti, S. Photoexcited Energy Transfer in a Weakly Coupled Dimer. *J. Phys. Chem. B* **2015**, *119*, 7242−7252.
(90) Ondarse-Alvarez, D.; Kömürlü, S.; Roitberg, A. E.; Pierdominici-Sottile, G.; Tretiak, S.; Fernandez-Alberti, S.; Kleiman, V. D. Ultrafast Electronic Energy Relaxation in a Conjugated Dendrimer Leading to Inter-Branch Energy Redistribution. *Phys. Chem. Chem. Phys.* **2016**, *18*, 25080−25089.
(91) Galindo, J. F.; Atas, E.; Altan, A.; Kuroda, D. G.; Fernandez-Alberti, S.; Tretiak, S.; Roitberg, A. E.; Kleiman, V. D. Dynamics of Energy Transfer in a Conjugated Dendrimer Driven by Ultrafast Localization of Excitations. *J. Am. Chem. Soc.* **2015**, *137*, 11637−11644.
(92) Fernandez-Alberti, S.; Roitberg, A. E.; Kleiman, V. D.; Nelson, T.; Tretiak, S. Shishiodoshi Unidirectional Energy Transfer Mechanism in Phenylene Ethynylene Dendrimers. *J. Chem. Phys.* **2012**, *137*, 22A526.
(93) Soler, M. A.; Roitberg, A. E.; Nelson, T.; Tretiak, S.; Fernandez-Alberti, S. Analysis of State-Specific Vibrations Coupled to the Unidirectional Energy Transfer in Conjugated Dendrimers. *J. Phys. Chem. A* **2012**, *116*, 9802−9810.
(94) Ondarse-Alvarez, D.; Oldani, N.; Roitberg, A. E.; Kleiman, V.; Tretiak, S.; FernandezAlberti, S. Energy transfer and spatial scrambling of an exciton in a conjugated dendrimer. *Phys. Chem. Chem. Phys.* **2018**, *20*, 29648−29660.
(95) Zheng, F.; Fernandez-Alberti, S.; Tretiak, S.; Zhao, Y. Photoinduced Intra- and Intermolecular Energy Transfer in Chlorophyll a Dimer. *J. Phys. Chem. B* **2017**, *121*, 5331−5339.
(96) Greenfield, M. T.; McGrane, S. D.; Bolme, C. A.; Bjorgaard, J. A.; Nelson, T. R.; Tretiak, S.; Scharff, R. J. Photoactive high explosives: linear and nonlinear photochemistry of petrin tetrazine chloride. *J. Phys. Chem. A* **2015**, *119*, 4846−4855.
(97) Nelson, T.; Bjorgaard, J.; Greenfield, M.; Bolme, C.; Brown, K.; McGrane, S.; Scharff, R. J.; Tretiak, S. Ultrafast Photodissociation Dynamics of Nitromethane. *J. Phys. Chem. A* **2016**, *120*, 519−526.
(98) Lystrom, L.; Zhang, Y.; Tretiak, S.; Nelson, T. Site-Specific Photodecomposition in Conjugated Energetic Materials. *J. Phys. Chem. A* **2018**, *122*, 6055−6061.
(99) Sifain, A. E.; Gifford, B. J.; Gao, D. W.; Lystrom, L.; Nelson, T. R.; Tretiak, S. NEXMD Modeling of Photoisomerization Dynamics of 4-Styrylquinoline. *J. Phys. Chem. A* **2018**, *122*, 9403−9411.
(100) Nelson, T.; Fernandez-Alberti, S.; Chernyak, V.; Roitberg, A. E.; Tretiak, S. Nonadiabatic Excited-State Molecular Dynamics Modeling of Photoinduced Dynamics in Conjugated Molecules. *J. Phys. Chem. B* **2011**, *115*, 5402−5414.
(101) Nelson, T.; Fernandez-Alberti, S.; Chernyak, V.; Roitberg, A.; Tretiak, S. Nonadiabatic Excited-State Molecular Dynamics: Numerical Tests of Convergence and Parameters. *J. Chem. Phys.* **2012**, *136*, No. 054108.
(102) Bjorgaard, J. A.; Kuzmenko, V.; Velizhanin, K. A.; Tretiak, S. Solvent effects in timedependent self-consistent field methods. I. Optical response calculations. *J. Chem. Phys.* **2015**, *142*, No. 044103.
(103) Bjorgaard, J. A.; Velizhanin, K. A.; Tretiak, S. Solvent effects in time-dependent self-consistent field methods. II. Variational formulations and analytical gradients. *J. Chem. Phys.* **2015**, *143*, No. 054305.
(104) Bjorgaard, J. A.; Nelson, T.; Kalinin, K.; Kuzmenko, V.; Velizhanin, K. A.; Tretiak, S. Simulations of fluorescence solvatochromism in substituted PPV oligomers from excited state molecular dynamics with implicit solvent. *Chem. Phys. Lett.* **2015**, *631-632*, 66−69.
(105) Fernandez-Alberti, S.; Kleiman, V. D.; Tretiak, S.; Roitberg, A. E. Nonadiabatic Molecular Dynamics Simulations of the Energy Transfer between Building Blocks in a Phenylene Ethynylene Dendrimer. *J. Phys. Chem. A* **2009**, *113*, 7535−7542.
(106) Walker, R. C.; Crowley, M. F.; Case, D. A. The implementation of a fast and accurate QM/MM potential method in Amber. *J. Comput. Chem.* **2008**, *29*, 1019−1031.
(107) Dewar, M. J. S.; Zoebisch, E. G.; Healy, E. F.; Stewart, J. J. P. The development and use of quantum mechanical molecular models. 76. AMI: a new general purpose quantum mechanical molecular model. *J. Am. Chem. Soc.* **1985**, *107*, 3902.
(108) Stewart, J. J. P. Optimization of parameters for semiempirical methods I. Method. *J. Comput. Chem.* **1989**, *10*, 209−220.
(109) Dewar, M. J. S.; Thiel, W. Ground states of molecules. 38. The MNDO method, approximations and parameters. *J. Am. Chem. Soc.* **1977**, *99*, 4899−4907.
(110) Stewart, J. J. P. Optimization of parameters for semiempirical methods V: Modification of NDDO approximations and application to 70 elements. *J. Mol. Model.* **1999**, *13*, 1173−1213.
(111) Mukamel, S.; Tretiak, S.; Wagersreiter, T.; Chernyak, V. Electronic Coherence and Collective Optical Excitations of Conjugated Molecules. *Science* **1997**, *277*, 781−787.
(112) Tretiak, S.; Mukamel, S. Density Matrix Analysis and Simulation of Electronic Excitations in Conjugated and Aggregated Molecules. *Chem. Rev.* **2002**, *102*, 3171−3212.
(113) Davidson, E. R. *Reduced Density Matrices in Quantum Chemistry*; Academic Press: New York, 1976.
(114) Davidson, E. R. The Iterative Calculation of a Few of the Lowest Eigenvalues and Corresponding Eigenvectors of Large Real-Symmetric Matrices. *J. Comput. Phys.* **1975**, *17*, 87−94.
(115) Stratmann, R. E.; Scuseria, G. E.; Frisch, M. J. An efficient implementation of time-dependent density-functional theory for the calculation of excitation energies of large molecules. *J. Chem. Phys.* **1998**, *109*, 8218−8224.
(116) Chernyak, V.; Schulz, M. F.; Mukamel, S.; Tretiak, S.; Tsiper, E. V. Krylov-space algorithms for time-dependent Hartree-Fock and density functional computations. *J. Chem. Phys* **2000**, *113*, 36−43.
(117) Tretiak, S.; Isborn, C. M.; Niklasson, A. M. N.; Challacombe, M. Representation Independent Algorithms for Molecular Response Calculations in Time-Dependent Self-Consistent Field Theories. *J. Chem. Phys.* **2009**, *130*, No. 054111.
(118) Liu, B. *The simultaneous expansion method for the iterative solution of several of the lowest eigenvalues and corresponding eigenvectors of large real-symmetric matrices*; Lawrence Berkeley Laboratory: Berkeley, CA, USA, 1978.
(119) Hellmann, H. *Einfuhrung in die Quantenchemie*; F. Deuticke: Leipzig, 1937.
(120) Feynman, R. P. Forces in Molecules. *Phys. Rev.* **1939**, *56*, 340−343.
(121) Park, Y. I.; Kuo, C.-Y.; Martinez, J. S.; Park, Y. S.; Postupna, O.; Zhugayevych, A.; Kim, S.; Park, J.; Tretiak, S.; Wang, H.-L. Tailored Electronic Structure and Optical Properties of Conjugated Systems through Aggregates and Dipole−Dipole Interactions. *ACS Appl. Mater. Interfaces* **2013**, *5*, 4685−4695.

https://dx.doi.org/10.1021/acs.jctc.0c00248
J. Chem. Theory Comput. 2020, 16, 5771−5783

(122) Lin, H.; Truhlar, D. G. QM/MM: what have we learned, where are we, and where do we go from here? *Theor. Chem. Acc.* **2007**, 117.
(123) Tapia, O.; Goscinski, O. Self-consistent Reaction Field Theory of Solvent Effects. *Mol. Phys.* **1975**, *29*, 1653−1661.
(124) Onsager, L. Electric moments of molecules in liquids. *J. Am. Chem. Soc.* **1936**, *58*, 1486−1493.
(125) Kirkwood, J. G. The Dielectric Polarization of Polar Liquids. *J. Chem. Phys.* **1939**, *7*, 911.
(126) Klamt, A.; Schüürmann, G. COSMO: a new approach to dielectric screening in solvents with explicit expressions for the screening energy and its gradient. *J. Chem. Soc. Perkin Trans.* **1993**, *2*, 799.
(127) Scalmani, G.; Frisch, M. J.; Mennucci, B.; Tomasi, J.; Cammi, R.; Barone, V. Geometries and properties of excited states in the gas phase and in solution: Theory and application of a time-dependent density functional theory polarizable continuum model. *J. Chem. Phys.* **2006**, *124*, No. 094107.
(128) Cammi, R.; Mennucci, B. Linear response theory for the polarizable continuum model. *J. Chem. Phys.* **1999**, *110*, 9877.
(129) Cossi, M.; Barone, V. Solvent effect on vertical electronic transitions by the polarizable continuum model. *J. Chem. Phys.* **2000**, *112*, 2427.
(130) Improta, R.; Scalmani, G.; Frisch, M. J.; Barone, V. Toward effective and reliable fluorescence energies in solution by a new state specific polarizable continuum model time dependent density functional theory approach. *J. Chem. Phys.* **2007**, *127*, No. 074504.
(131) Improta, R.; Barone, V.; Scalmani, G.; Frisch, M. J. A state-specific polarizable continuum model time dependent density functional theory method for excited state calculations in solution. *J. Chem. Phys.* **2006**, *125*, No. 054103.
(132) Marenich, A. V.; Cramer, C. J.; Truhlar, D. G.; Guido, C. A.; Mennucci, B.; Scalmani, G.; Frisch, M. J. Practical computation of electronic excitation in solution: vertical excitation model. *Chem. Sci.* **2011**, *2*, 2143−2161.
(133) Swope, W. C.; Andersen, H. C.; Berens, P. H.; Wilson, K. R. A computer simulation method for the calculation of equilibrium constants for the formation of physical clusters of molecules: Application to small water clusters. *J. Chem. Phys* **1982**, *76*, 637−649.
(134) Allen, M. P.; Tildesley, D. J. *Computer Simulation of Liquids*; Oxford University Press: USA, 1990.
(135) van Gunsteren, W. F.; Berendsen, H. J. C. Algorithms for brownian dynamics. *Mol. Phys.* **1982**, *45*, 637−647.
(136) Paterlini, M. G.; Ferguson, D. M. Constant temperature simulations using the Langevin equation with velocity Verlet integration. *Chem. Phys.* **1998**, *236*, 243−252.
(137) Press, W. H.; Teukolsky, S. A.; Flannery, B. P.; Vetterling, W. T. *Numerical Recipes in Fortran 77: the art of scientific computing*, 2nd ed.; Cambridge University Press: New York, 1996.
(138) Hammes-Schiffer, S.; Tully, J. C. Proton transfer in solution: Molecular dynamics with quantum transitions. *J. Chem. Phys.* **1994**, *101*, 4657−4667.
(139) Fabiano, E.; Keal, T. W.; Thiel, W. Implementation of surface hopping molecular dynamics using semiempirical methods. *Chem. Phys.* **2008**, *349*, 334−347.
(140) IMSL *MATH/LIBRARY Special Functions*; Visual Numerics, Inc.: Houston, TX, *USA*.
(141) Hull, T. E.; Enright, W. H.; Jackson, K. R. *User's guide for DVERK - A subroutine for solving non-stiff ODEs*; Technical Report 100, Department of Computer Science: University of Toronto: Canada, 1976.
(142) Domcke, W.; Yarkony, D. R. Role of conical intersections in molecular spectroscopy and photoinduced chemical dynamics. *Annu. Rev. Phys. Chem.* **2012**, *63*, 325−352.
(143) Wang, L.; Beljonne, D. Flexible Surface Hopping Approach to Model the Crossover from Hopping to Band-Like Transport in Organic Crystals. *J. Phys. Chem. Lett.* **2013**, *4*, 1888−1894.
(144) Wang, L.; Prezhdo, O. V. A Simple Solution to the Trivial Crossing Problem in Surface Hopping. *J. Phys. Chem. Lett.* **2014**, *5*, 713−719.
(145) Meek, G. A.; Levine, B. G. Evaluation of the Time-Derivative Coupling for Accurate Electronic State Transition Probabilities from Numerical Simulations. *J. Phys. Chem. Lett.* **2014**, *5*, 2351−2356.
(146) Meek, G. A.; Levine, B. G. Accurate and Efficient Evaluation of Transition Probabilities at Unavoided Crossings in Ab Initio Multiple Spawning. *Chem. Phys.* **2015**, *460*, 117−124.
(147) Granucci, G.; Persico, M.; Toniolo, M. Direct Semiclassical Simulation of Photochemical Processes with Semiempirical Wave Functions. *J. Chem. Phys.* **2001**, *114*, 10608−10615.
(148) Nelson, T. R.; White, A. J.; Bjorgaard, J. A.; Sifain, A. E.; Zhang, Y.; Nebgen, B.; FernandezAlberti, S.; Mozyrsky, D.; Roitberg, A. E.; Tretiak, S. Non-adiabatic Excited State Molecular Dynamics: theory and applications for modeling photophysics in extended molecular materials. *Chem. Rev.* **2020**, *120*, 2215−2287.
(149) Subotnik, J. E.; Jain, A.; Landry, B.; Petit, A.; Ouyang, W.; Bellonzi, N. Understanding the Surface Hopping View of Electronic Transitions and Decoherence. *Annu. Rev. Physiol.* **2016**, *67*, 387−417.
(150) Webster, F.; Wang, E. T.; Rossky, P. J.; Friesner, R. A. Stationary Phase Surface Hopping for Nonadiabatic Dynamics: Two-State Systems. *J. Chem. Phys.* **1994**, *100*, 4835−4847.
(151) Akimov, A. V.; Long, R.; Prezhdo, O. V. Coherence Penalty Functional: A Simple Method for Adding Decoherence in Ehrenfest Dynamics. *J. Chem. Phys.* **2014**, *140*, 194107.
(152) Jaegar, H. M.; Fischer, S.; Prezhdo, O. V. Decoherence-Induced Surface Hopping. *J. Chem. Phys.* **2012**, *137*, 22A545.
(153) Subotnik, J. E.; Ouyang, W.; Landry, B. R. Can We Derive Tully's Surface-Hopping Algorithm from the Semiclassical Quantum Liouville Equation? Almost, but Only with Decoherence. *J. Chem. Phys.* **2013**, *139*, 214107.
(154) Ouyang, W.; Subotnik, J. E. Estimating the Entropy and Quantifying the Impurity of a Swarm of Surface-Hopping Trajectories: A New Perspective on Decoherence. *J. Chem. Phys.* **2014**, *140*, 204102.
(155) Landry, B. R.; Subotnik, J. E. How to Recover Marcus Theory with Fewest Switches Surface Hopping: Add Just a Touch of Decoherence. *J. Chem. Phys.* **2012**, *137*, 22A513.
(156) Tully, J. C. Perspective: Nonadiabatic dynamics theory. *J. Chem. Phys.* **2012**, *137*, 22A301.
(157) Hack, M. D.; Truhlar, D. G. A Natural Decay of Mixing Algorithm for NonBorn−Oppenheimer Trajectories. *J. Chem. Phys.* **2001**, *114*, 9305−9314.
(158) Granucci, G.; Persico, M.; Zoccante, A. Including Quantum Decoherence in Surface Hopping. *J. Chem. Phys.* **2010**, *133*, 134111.
(159) Bjorgaard, J. A.; Sheppard, D.; Tretiak, S.; Niklasson, A. M. N. Extended Lagrangian Excited State Molecular Dynamics. *J. Chem. Theory and Comp.* **2018**, *14*, 799−806.
(160) Barbatti, M.; Sen, K. Effects of Different Initial Condition Samplings on Photodynamics and Spectrum of Pyrrole. *Int. J. Quantum Chem.* **2016**, *116*, 762−771.
(161) Sindhikara, D. J.; Kim, S.; Voter, A. F.; Roitberg, A. E. Bad Seeds Sprout Perilous Dynamics: Stochastic Thermostat Induced Trajectory Synchronization in Biomolecules. *J. Chem. Theory Comput.* **2009**, *5*, 1624−1631.
(162) Fernandez-Alberti, S.; Kleiman, V. D.; Tretiak, S.; Roitberg, A. E. Unidirectional Energy Transfer in Conjugated Molecules: The Crucial Role of High-Frequency C≡C Bonds. *J. Phys. Chem. Lett.* **2010**, *1*, 2699−2704.
(163) Freixas, V. M.; Fernandez-Alberti, S.; Makhov, D. V.; Tretiak, S.; Shalashilin, D. An *ab initio* multiple cloning approach for the simulation of photoinduced dynamics in conjugated molecules. *Phys. Chem. Chem. Phys.* **2018**, *20*, 17762−17772.

https://dx.doi.org/10.1021/acs.jctc.0c00248
J. Chem. Theory Comput. 2020, 16, 5771−5783